16th Australasian Fluid Mechanics Conference
Crown Plaza, Gold Coast, Australia
2-7 December 2007

Impulse Evaluation by a Force Transmitting Device in a Blast Environment

A.D. Resnyansky and S.A. Weckert

Weapons Systems Division
Defence Science and Technology Organisation, Edinburgh, South Australia, 5111 AUSTRALIA

Abstract

An alternative to traditional momentum pendulum and pressure gauges is considered to resolve an improved temporal response to blast and fragmentation, with a protected gauge design. An alternative design based on the use of strain gauges is suggested. A gas gun fitted with a diverging nozzle has been used to validate a version of the system. Numerical analysis has been performed to explore and assess the accuracy of the experimental validation process and indicates an appropriate time range for the validation data. The test and simulation results demonstrate the potential of this device for measurement of blast and fragmentation effects.

Introduction

Accurate measurement of momentum due to blast and fragmentation is important for assessing threats such as Improvised Explosive Devices (IEDs). One particular measurement technique involves a strain gauge instrumented rod and has several advantages over other methods. It is capable of measuring the momentum due to both blast and fragments whereas pressure gauges can only measure blast. It is robust and resistant to damage, making it suitable for close-range and fragmentation environments. It can provide temporal resolution of the effects which free moving masses lack, and does not have the processing errors associated with the differentiation of recorded displacement for transducer based systems, such as that presented in [1]. The instrumented rod has been used successfully for close-range, short duration measurements in [2], however the measurement time was restricted by the length of the rod. The technique has been further developed in [3] to allow for measurement of longer duration events, where numerous wave reflections and interactions occur in the rod during the loading period. The oscillations due to these wave circulations were effectively reduced while maintaining a good correlation between the momentum of the output signal and the input load.

For calibration of the Momentum Measurement Device (MMD) developed in [3], a gas gun has been used to impart a high pressure load to the Momentum Gauge. In order to achieve a sufficiently high pressure, the MMD is required to be in close proximity to the gas gun muzzle. However, the flow in this region is complicated and due to the reactive nature of the device, the dynamic pressure component of the flow affects the force measured by the device. Therefore, flow around the active element of the MMD can also influence the results. In order to minimize spatial inhomogeneities, a diverging nozzle has been used in addition to a standard constant diameter barrel. However, the load level is reduced when using the nozzle. The present work investigates the influence of the flow effects on the accuracy of the results produced using the device developed in [3]. These effects have been analysed numerically using the IFSAS-II CFD code [4] and the CTH hydrocode [5].

Set-Ups for Momentum Gauge and Experiments

A schematic of the MMD and the experimental set-up used in [3], which forms the basis of the present work, is shown in Fig.1.

A gas gun fitted with either a 10 mm diameter barrel or a diverging nozzle N, was used to produce the pressure pulse for evaluating the device. The pressure pulse is incident on the front plate F of the device, which amplifies the force transmitted to the rod R. The rod is instrumented with strain gauges G and has a large mass M attached at the rear via a damper element D, which minimises the system oscillations. The diameter of the MMD front plate was chosen to be 160 mm, and the exit diameter of the 60 cm long diverging nozzle is 180 mm.

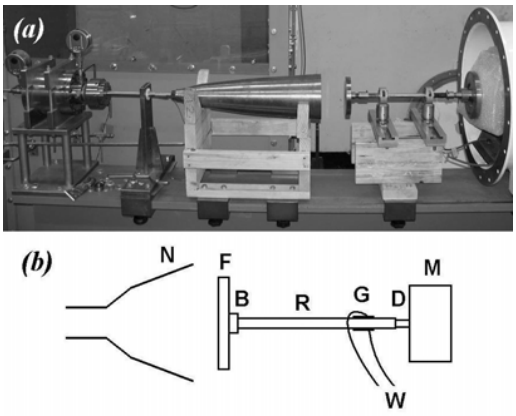

Figure 1. The experimental set-up (a) and a schematic of the device (b).

For the pressure measurement set-up a 250 mm diameter solid steel mounting plate was used, with one pressure gauge mounted directly opposite the centre of barrel/nozzle (along the symmetry axis, r = 0), and two other gauges positioned at r = 40 and 80 mm. A 10 cm stand-off distance between the barrel/nozzle and the target plate (pressure gauge plate or MMD front plate) has been used for the experimental and simulation set-ups.

Numerical Analysis

The gas flow produced at the exit of the barrel and nozzle has been studied and is a complex process of shock and rarefaction wave interactions during the gas expansion.

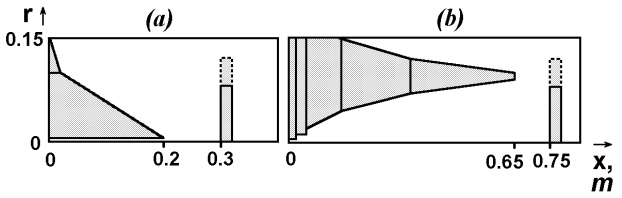

Figure 2. Numerical set-ups for the IFSAS-II modelling of gas flow from the barrel (a) and the diverging nozzle (b).

The numerical two-dimensional axi-symmetric set-ups considered with IFSAS-II are shown in Fig 2. Inflow into the area forming the barrel/nozzle was set at 100 atm (10 MPa) pressure at the x=0 boundary. The 16 cm diameter MMD front plate is shown by the solid rectangle in Fig. 2 and the 25 cm

diameter pressure gauge mounting plate is shown by the dashed extension of the rectangle. The complexity of the flow can be illustrated by the pressure profile along the symmetry axis. Examples of the pressure profile for the set-ups (a) and (b) in Fig. 2 are shown in Fig. 3 at the time instants when the shock wave is approaching the target plate. Pressure profile 2 in Fig. 3(a) illustrates the equilibrating of the flow at the condition of constant inflow. The pressure drop below 10 MPa inside the barrel occurs due to the rarefaction travelling back from the muzzle exit into the barrel. Obviously, the results will depend on the barrel length (in the physical tests it is more than 1 m); however, we do not try to simulate directly the test but to assess the contributing factors in the test records.

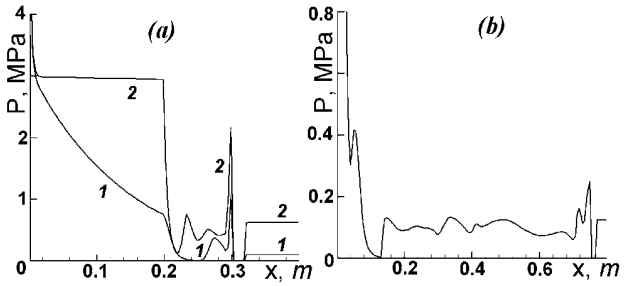

Figure 3. IFSAS-II calculated pressure variation along the symmetry axis for the barrel (a) t=0.6ms (*1*) and 56 ms (*2*) and for the nozzle (b) t=2ms.

In order to evaluate the load on the target plate due to the gas flow from the barrel, the static pressure was calculated 10 cm from the barrel exit using the CTH hydrocode. The CTH set-up for the barrel configuration was similar to Fig. 2(a); however, the target plate was not included and the barrel was modelled with an infinite thickness to avoid any deformation or leakage problems The CTH hydrocode is not designed for CFD problems, therefore, the simulation time was limited to only a few milliseconds due to code cell thermodynamics issues. However, the calculation results shown in Fig. 4 confirm that for the initial loading stage there is significant pressure variation depending on the location of the gauge from the symmetry axis.

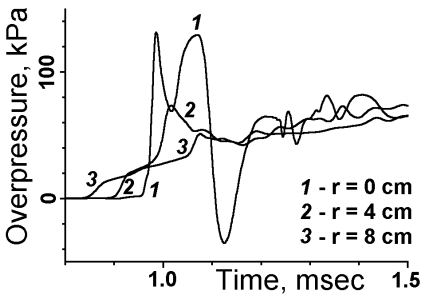

Figure 4. CTH calculation - pressure distribution over the target plate for the barrel set-up.

It can be seen in Fig. 4 that after the initial loading period, the pressure appears to equilibrate and become spatially uniform, however, this is likely to be caused by wave reflections from the solid sections of the infinite thickness muzzle. Additionally, during the initial loading period, the pressure precursors for the peripheral gauges arrive earlier (curve 3 then 2) than the central gauge. This is explained by high-speed transfer of the load via the barrel section of the computation domain, followed by lateral boundary condition effects that are not soft enough in the hydrocode for a CFD simulation. In order to model the experimental set-up with greater fidelity, the next calculation was conducted with IFSAS-II using the set-up from Fig. 2(a). Code restrictions prevented complete elimination of the reflecting solid boundaries from the section representing the barrel, however, the IFSAS-II model gave an improved representation of the experimental set-up to allow insight into the major features of the flow. The calculation results in Fig. 5 represent pressure traces at the gauge locations G1, G2, and G3 corresponding to r=0, 4, and 8 cm immediately in front of the target plate facing the inflow.

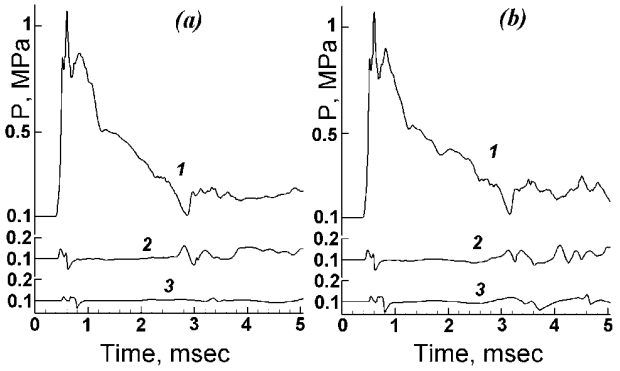

Figure 5. IFSAS-II calculated pressure traces at the gauge locations for the barrel set-up with a 16cm- (a) and a 25cm-diameter (b) target plate.

A comparison of the results of Fig 5(a) and (b) indicates that the plate diameter has a negligible effect on the initial stage of loading, with similar spatially non-uniform pressure distributions for both cases. The experimental pressure records for gauges mounted on the 250 mm diameter plate are shown in Fig. 7 for the initial stage of loading. This pressure distribution evaluated at r = 0 cm (1), r = 4 cm (2) and r = 8 cm (3) shows a similar spatial non-uniformity, with a high pressure at the centre gauge location and lower pressures at the peripheral positions.

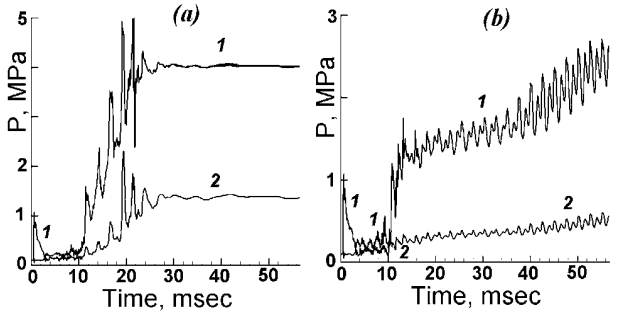

Figure 6. IFSAS-II calculated pressure traces for gauge locations G1 and G2 for the barrel with a 16cm- (*a*) and 25cm-diameter (*b*) target plate.

The pressure traces presented in Fig. 5 are representative for the time duration comparable with the initial stage of flow around the target plate.

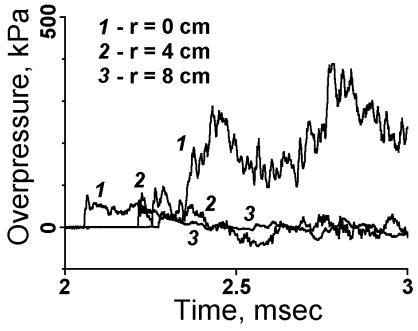

Figure 7. Experimental pressure data from gauges G1, G2, and G3 for the flow from the barrel against a 25cm-diameter plate.

However, a more complicated process is observed at a later time (Fig. 6), which is associated with the pressure build up in the region between the muzzle and the target plate. A similar loading behaviour is observed in the experimental data where after initial peak and drop due to the release at the muzzle, the pressure begins to build up and continue at this level as evident in the longer experimental record of Fig. 8. At the same time, the peripheral gauges, G2 and G3, demonstrate a quick release of pressure, which continues for the whole record length. The non-uniformity is emphasised to a greater degree by the full record (1sec) from the experimental data, where the pressure and the impulse ($I = \int pdt$) are shown in Figs. 8 and 9 respectively.

Conversely, the numerical results for the r = 4 cm peripheral gauge (curve 2 in Fig. 6) show a slow pressure build up that can be explained by the boundary restriction from the barrel construction in the model (the presence of inclined wedge is necessary for the required inflow boundary conditions in IFSAS-II). This restriction slows down the pressure release as compared to that observed in the experimental data. Numerical data for the location at G3 (not shown) is also very close to curve 2 (G2) in Fig. 6, which also confirms the fact of the prevailing boundary condition on the load in this set-up.

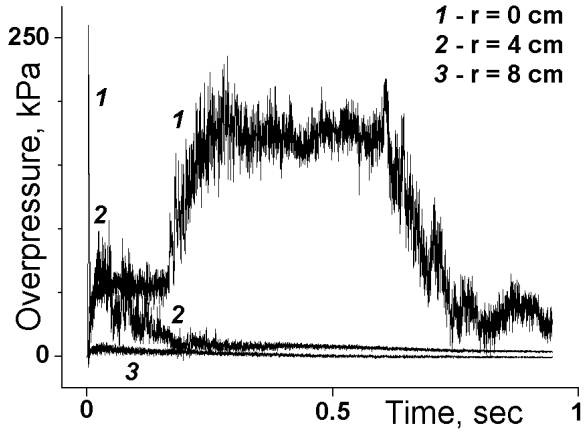

Figure 8. Experimental pressure data (extended) from gauges G1, G2, and G3 for the flow from the barrel against a 25cm-diameter plate.

As follows from the numerical and experimental analysis conducted in Figs. 4-8, the pressure build up is determined by the environment surrounding the test site. This environment in the numerical set-up is represented by the muzzle configurations; as a result, the pressure build up starts almost directly after the initial stage of loading in the CTH modelling (Fig. 4) and approximately after 10 msec in the IFSAS-II modelling (Fig. 6).

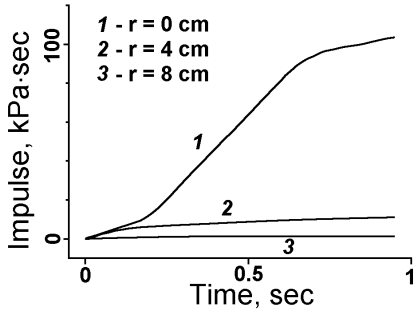

Figure 9. Experimental data (impulse) from gauges G1, G2, and G3 for the flow from the barrel against a 25cm-diameter plate.

In the experimental testing, the boundary restrictions were more remote in the test site environment, and thus the pressure build up shown in Fig. 8 is delayed until approximately 200msec. The build up is also reflected by the noticeable impulse rise at this time for the gauge location G1 shown in Fig. 9. The impulse data shows a negligible impulse at gauge G3 as compared to the impulse for gauges G1 and G2, with the latter quite similar in their response until approximately 200msec.

A diverging nozzle was designed using the CTH hydrocode [5] (Sandia National Laboratories) to improve the spatial distribution of the pressure pulse over the front plate of the gauge. The calculation results shown in Fig. 10 give the pressure distribution at r=0cm (1), r=4cm (2) and r=8cm (3) for initial part of the pulse.

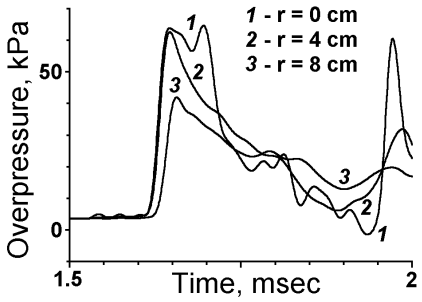

Figure 10. CTH calculation - pressure distribution over the target plate for the diverging nozzle set-up

To analyse the process for a longer period of time, IFSAS-II was used again to model the flow through the nozzle and around the target plate.

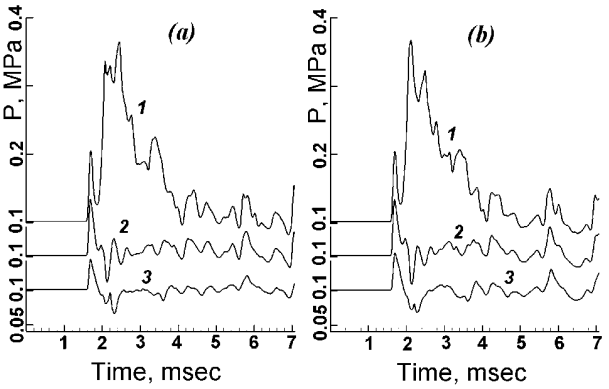

Figure 11. IFSAS-II calculated pressure traces at the gauge locations for the flow from the nozzle against the 16cm- (a) and 25cm-diameter (b) target plates.

The numerical analysis results shown in Fig. 11 demonstrate that prior to the pressure build up, the pressure pulses are quite similar for the 16cm- and 25cm-diameter target plates. Therefore, the pulses can be used for calibration within this timeframe of the flow process.

The experimental results shown in Fig. 12 confirm that the pressure data are quite similar for all three gauges; therefore, the pressure pulse is fairly uniform over the plate area. The impulse ($I = \int pdt$) for an increased record length (1sec) is shown for the experimental data in Fig. 13 and indicates some degree of non-uniformity with less impulse at the 8cm radial location. However,

the non-uniformity is much less than that observed for the barrel case (Fig. 9).

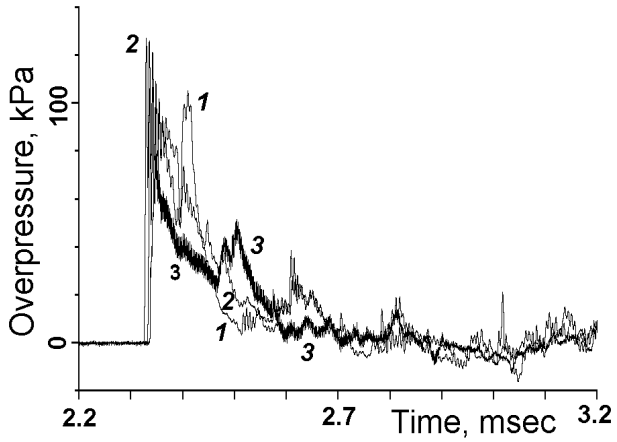

Figure 12. Experimental pressure data from gauges G1, G2, and G3 for the flow from the nozzle against a 25cm-diameter plate.

A low gradient variation in impulse after 0.5s from the gauges (Fig. 13) can be explained by gauge zero-shift.

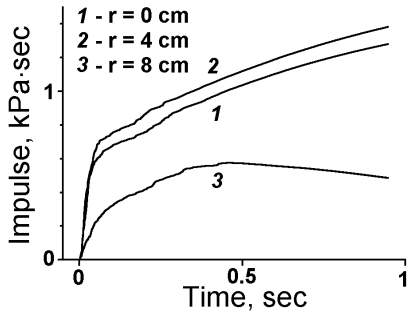

Figure 13. Experimental data (impulse) from gauges G1, G2, and G3 for the flow from the nozzle against a 25cm-diameter plate.

A similar pressure build up at approximately 160msec was also observed in the experimental data for the nozzle set-up.

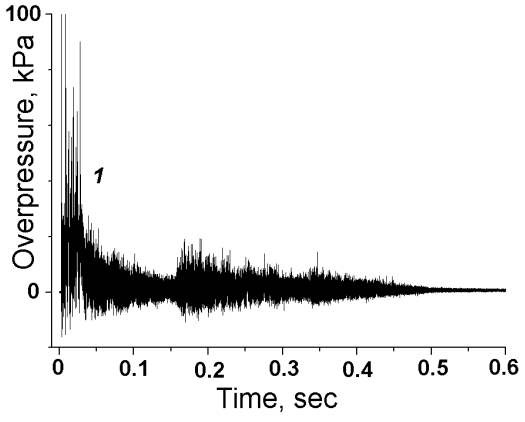

Figure 14. Experimental pressure data (extended) from gauge G1 for the flow from the nozzle against a 25cm-diameter plate.

This is shown in Fig 14 for the central gauge G1, and confirms the influence of the boundary restrictions in the test site environment.

Conclusion and Discussion

The present analysis has demonstrated that the process of loading the target plate supporting the pressure gauges or the front plate of the MMD is characterised by an initial stage of loading followed by pressure release and a pressure build up dictated by the site configuration (boundary conditions). It has been shown numerically that the stages of peak loading and subsequent release are only slightly affected by the target plate dimensions. Thus the loading conditions are very similar for the Momentum Gauge and pressure gauge experimental set-ups where the momentum gauge uses a 16cm-diameter front plate and the pressure gauges are mounted on a larger 25cm-diamter plate. This allows us to confidently compare the momentum data obtained from the experimental pressure records with the momentum from the experimental MMD data. The barrel loading introduces a significant non-uniformity over the target plate that is confirmed both numerically and experimentally, with good agreement between the two. This non-uniformity makes it difficult to accurately integrate the pressure over the plate with only three gauge locations. The nozzle loading provides a comparatively spatially homogeneous loading profile which improves the accuracy of the pressure integration over the plate.

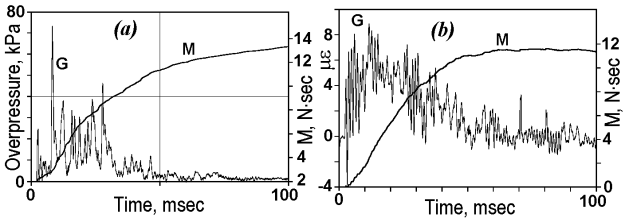

Figure 15. Experimental load and momentum data taken from the pressure gauge set-up (*a*) and MMD (*b*).

The efficacy of the MMD is confirmed in the calibration process where the momentum from the experimental pressure gauge data is compared to that obtained from the MMD. The results are shown in Fig. 15 where the time duration is limited to 100msec to provide an appropriate pulse duration prior to the pressure build up. The pressure gauge data, shown in Fig. 15(a), was integrated over the front plate area, assuming linear pressure variation between the radial measurement locations, to obtain the force and corresponding momentum (curve M). Independently the momentum was calculated from the MMD data where Fig. 15(b) shows the strain gauge data in microstrain (curve G) and the corresponding momentum (curve M). A comparison of the results from Fig. 15(a) and (b) indicates reasonable agreement and demonstrates the potential of this measurement device.

References

[1] Clemedson, C.-J & Jönsson, A., A transducer for recording mechanical impulse with special application to air blast research, *J. of Physics E: Scientific Instruments*, **3**, 1970, 180-184.

[2] Edwards, D.H. et al., Blast wave measurements close to explosive charges, *Shock Waves*, **2**, 1992, 237-243.

[3] Resnyansky, A.D. & Weckert, S.A., Experimental and theoretical assessment of a device used for evaluation of blast and fragmentation effects, Proceedings of the 15th APS Topical Conference on Shock Compression of Condensed Matter, Hawaii, 2007.

[4] IFSAS-II User Manual, Martec Ltd., Halifax, NS, Canada, 2002.

[5] Bell R.L., Baer M.R., Brannon R.M., Crawford D.A., Elrick M.G., Hertel, Jr. E.S., Schmitt R.G., Silling S.A., and Taylor P.A., CTH User's Manual and Input Instructions, Version 7.1 (Internal Report), CTH Development Project, Sandia National Laboratories, Albuquerque, NM, 2006.